Photocatalytic removal of NOx over immobilized BiFeO₃ nanoparticles and effect of operational parameters

Taher Rahimi Aghdam*, Habib Mehrizadeh**, Dariush Salari*,†, Hui-Hsin Tseng***,
Aligholi Niaei****, and Azam Amini*

*Research Laboratory of Petroleum Technology, Faculty of Chemistry, University of Tabriz, Tabriz, Iran
**Department of Applied Chemistry, Faculty of Chemistry, University of Urmia, Urmia, Iran
***School of Occupational Safety and Health, Chung Shan Medical University, Taichung, 402, Taiwan, ROC
****Research Laboratory of Reactor and Catalyst, Faculty of Chemical Engineering, University of Tabriz, Tabriz, Iran

Abstract−Perovskite type BiFeO₃ (BFO) was synthesized by sol-gel auto-combustion method. Synthesized BFO was immobilized on the micro slides glass plates by sol-gel dip-coating method. The sample was characterized by XRD, FESEM, UV-Vis DRS, and BET techniques. The XRD pattern confirmed the perovskite structure, and from the Debye-Scherrer equation the average crystalline size was calculated as 19 nm. The FE-SEM images of prepared BFO showed porous structure with low agglomeration. The band gap energy was calculated about 2.13 eV, and the specific surface area (SSA) of prepared BFO nanostructure was obtained 55.1 m² g⁻¹. The photocatalytic activity of prepared pure and immobilized BFO was investigated in the removal of NOx under UV irradiation, in the batch photoreactor. The effects of operational parameters such as initial concentration of NOx, light intensity and amount of coated photocatalyst, under identical conditions, were investigated. The results showed that the highest conversion of NOx was obtained as 35.83% in the 5 ppm of NOx with 1.2 g immobilized BFO and under 15 W illumination lamp.

Keywords: Air Pollution, Photocatalysis, Perovskite, Nanostructure, Bismuth Ferrite
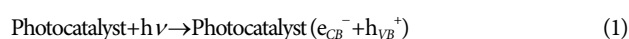
INTRODUCTION

Urban air pollutants, mainly including NOx, SOx, and VOCs, are one of the most important problems that humans are facing in today's life. These pollutants are generated from natural (e.g., volcanic eruptions etc.) and anthropogenic sources (exhaust gases and so on) and have negative impacts on human health, animal life, plants and climate change on the global scale [1]. The most common nitrogen oxides are nitrogen monoxide (NO) and nitrogen dioxide (NO₂) (both are called NOx), which are emitted from both combustion and natural sources [2]. High levels of NOx are causing various environmental and health problems such as acid rain, visibility reduction, greenhouse effect, ecological toxification and human diseases [2]. Thus, it is necessary to control and/or remove such pollutants. There are two main procedures to remove NOx, including primary and secondary methods [3]. Whereas primary methods, such as fuel staging and air staging [3], focus on the reducing NOx production, secondary methods are applied to remove NOx after emission. Selective catalytic reduction (SCR) [4], selective non-catalytic reduction (SNCR) [5], NOx storage and reduction (NSR) [3], absorption of NOx, and photo-processes are the most common secondary methods [2]. Among these, photodecomposition, using heterogeneous semiconductor photocatalysts, is a promising and sustainable technology for the photodecompo-

sition of NOx to benign N₂ and O₂ under mild conditions [6].

BiFeO₃ (BFO) is a promising photocatalyst with small band gap energy (2.1-2.8 eV) [7] and high chemical stability, which uses as a semiconductor in various applications such as photocatalyst to remove environmental pollutants [7,8]. Ai and coworkers [9] reported the synthesis of ternary bismuth oxybromide (BiOBr) crystalline nanoplate by nonaqueous sol-gel method and studied the removal of low concentration of NO (400 ppb) by synthesized photocatalyst under 300 W UV and visible light irradiation.

When photons with suitable energy come onto the BFO, electrons (e⁻) and holes (h⁺) are generated due to the electron excitation from valance band to conduction band. These species are very reactive and can either recombine or diffuse to the semiconductor surface, reacting with adsorbed species, such as pollutants, water, oxygen. Thus, pollutants can be removed either directly by e⁻ and/or h⁺ or indirectly by hydroxyl, superoxide and/or other reactive radicals have formed from adsorbed water and oxygen [10]. Along this, the ferroelectric properties of BFO with spontaneous polarization enhance the photoinduced electron-hole separation efficiency and thus increase the photocatalytic activity of BFO [11].

Some mechanisms have been proposed for NO photodecomposition on various photocatalysts [12-15]. Bowering et al. [12] listed the following reactions for nitric oxides photodecomposition:

$$\text{Photocatalyst} + h\nu \rightarrow \text{Photocatalyst}\,(e_{CB}^- + h_{VB}^+) \tag{1}$$

$$\text{NO}_{(ads)} + e_{CB}^- \rightarrow \text{N}_{(ads)} + \text{O}_{(ads)} \tag{2}$$

$$\text{NO}_{(ads)} + \text{N}_{(ads)} \rightarrow \text{N}_2\text{O}_{(ads)} \tag{3}$$

$$2N_{(ads)} \rightarrow N_2 (g) \tag{4}$$

$$2NO_{(ads)} \rightarrow N_2 (g) + O_2 (g) \tag{5}$$

$$2N_2O_{(ads)} \rightarrow 2N_2 (g) + O_2 (g) \tag{6}$$

Generally, NO photodecomposition can be conveniently divided into sequential steps, all of which impact the reaction efficiency. First, reactants, NO and O_2 for example, adsorb on photocatalyst surface. In the next stage of photocatalytic cycle, photoinduced electron-hole are generated by irradiating light containing photon with energy more than band gap energy. Absorbed species react with each other, in the third step, and new absorbed species are formed. Finally, gas desorption takes place and the cycle is completed [16,17].

In this work, for effective removal of high concentration of NOx pollutant by BFO and study the effective operational parameters in photocatalytic removal of NOx, perovskite type BFO was synthesized by sol-gel auto-combustion method. Synthesized BFO was immobilized on the micro slides glass plates by sol-gel dip-coating method and their photocatalytic activity in the removal of NO pollutants under UV irradiation in the annular photoreactor was studied. The sample was characterized by XRD, SEM, UV-Vis DRS, and BET techniques. The effects of operational parameters such as initial concentration of NO, light intensity, as well as, catalyst loading were studied.

EXPERIMENTAL

1. Materials

$Bi(NO_3)_3 \cdot 5H_2O$, $Fe(NO_3)_3 \cdot 9H_2O$, citric acid ($C_6H_8O_7 \cdot H_2O$), methyl-trimethoxysilane ($CH_3Si(OCH_3)_3$), methanol, HCl, HNO_3 and NaOH were purchased from Merck, Germany. The micro slides glass plates ($1.2 \times 25.4 \times 76.2$ mm) as a substrate to immobilize the prepared photocatalyst were obtained from Sail Brand, China.

2. Preparation of BFO Nanoparticles

The BFO nanoparticles were synthesized by sol-gel auto-combustion method. In a typical procedure, 10 mmol $Bi(NO_3)_3$ and 10 ml HNO_3 (65% v/v) were added into 200 ml distilled water at the 500 ml glass beaker. The mixture was stirred magnetically to obtain a transparent solution. Then 10 mmol $Fe(NO_3)_3$ was added to above solution, followed by 20 min magnetic stirring at 70 °C. After that, 20 g citric acid was added and magnetic stirring continued for 2 h in 90 °C. Polycondensation reactions between nitrate ions and citric acid were carried out during the dehydration process and caused the formation of a gel. When the gel was formed, the temperature was raised to 200 °C to burn the organic content and the reaction products converted into the brownish red powder. The prepared powder was calcined in air at 700 °C for 5 h, to decompose the organic part (i.e., citrate compounds) and cooled naturally to room temperature and finally stored for applications.

3. Immobilization of Prepared BFO on the Glass Plates

Synthesized BFO was immobilized on the micro slides glass plates by sol-gel dip-coating method. Methyltrimethoxysilane was used as a binder. To get a uniform coating, pre-treatment was carried out by soaking the glass micro slides plates in 2 M NaOH solution for 2 h, followed by drying at 50 °C for 2 h. The coating mixture composed of 60 ml methanol, 20 ml HCl (1 M), 5 ml methyltrimethoxysilane, and 2.5 g of photocatalyst nanoparticles, was stirred for 2 h to form uniform dispersion. 6 micro slides glass plates were dipped simultaneously into the dispersed mixture of photocatalyst
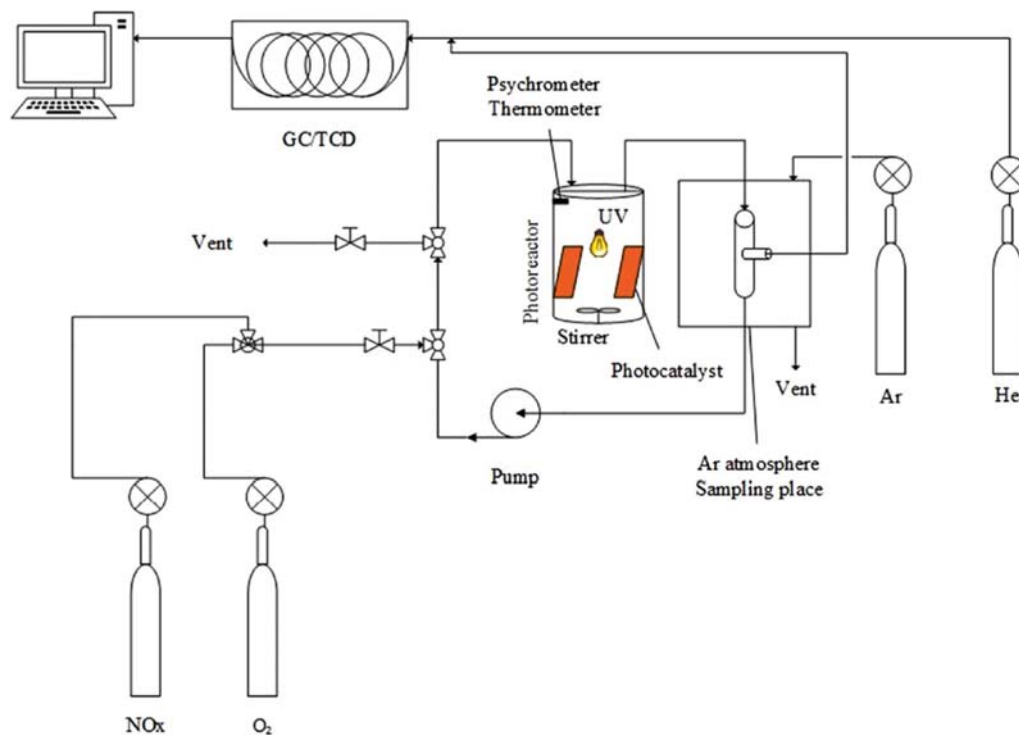

Fig. 1. The designed set-up for the photocatalytic removal of NOx.

for 3 min and then withdrawn manually in 20 seconds to form stable immobilized photocatalyst. The films were dried at room temperature (30 °C) for 4 h to produce chemical bonds between the deposited BFO and the plate. For more densification of the films, all the immobilized plates were thermally cured at 100 °C for 1 hour. To increase the density of immobilized photocatalyst, the process was repeated. At the end of this procedure, weight deference between bare and immobilized glass plate was about 0.2 g that was mainly attributed to the immobilized BFO. In comparison to the films that made by the dried mixture of BFO and water, in the sol-gel dip-coating method, due to the formation of chemical bonding between BFO and the glass surface, the immobilized BFO sticks firmly to the glass surface [18].

4. Characterizations of Prepared BiFeO₃

To determine the crystal phase composition and average crystalline size of the BFO nanoparticles sample, X-ray diffraction (XRD) measurements were carried out at room temperature by using Siemens X-ray diffraction D5000, with Cu Kα radiation. The accelerating voltage of 40 kV and emission current of 30 mA were used. Surface morphology of samples was observed using field emission scanning electron microscopy (FE-SEM) (Mira3 FESEM, Tescan, Czech Republic). UV-Vis diffuse reflectance spectroscopy (UV-Vis DRS) (UV-Vis spectrophotometer: Hitachi, U-3900, Japan) was used to study the light response of prepared BFO nanoparticles and the band gap energy of prepared photocatalyst was determined based on DRS. The specific surface area and other surface properties were determined through BET analysis by a BET Sorptometer (PMI, BET-201-AEL, USA).

5. Photocatalytic Removal Process of NOx

The experimental set-up for study the photocatalytic activity of immobilized BFO nanoparticles on the glass plate is shown in Fig. 1. A self-designed annular batch photoreactor with the total volume of 1,500 cm³ was used to study the photocatalytic removal process of NO. To evaluate the photocatalytic activity, immobilized glass plates were installed on the inner wall of the photoreactor. Continuous flow of O_2 (200 ml min⁻¹) was passed through the photoreactor for 10 min to evacuate N_2 and then desired concentration of NO was mixed with O_2 in controlled humidity. To achieve homogeneous dispersion of gaseous molecules in the reactor, stirrer rotation was used in the photoreactor. A 15 W UV lamp (Philips, UV-C, The Netherlands) was inserted vertically in the quartz tube, which was located separately from the catalyst chamber at the center of the photoreactor. The temperature of the photoreactor was controlled by air stream inside the quartz tube. Photocatalytic removal process of NO started by lighting on the UV lamp and sampling from the reactor during irradiation time at the appropriate intervals. Sampling and GC injecting were carried out in Ar atmosphere to prevent N_2 entering into the Hamilton syringe. Quantitative analysis of samples was by GC/TCD (Shimadzu 2010 plus, HP-Mole sieve column: length 30 m, i.d. 0.53 mm, film thickness 25.00 μm) and the amount of N_2 was detected as a function of illumination time.

The overall reaction is given by Eq. (7):

$$2NO \rightarrow N_2 + O_2 \tag{7}$$

Therefore conversion of NO can be expressed as Eq. (8):
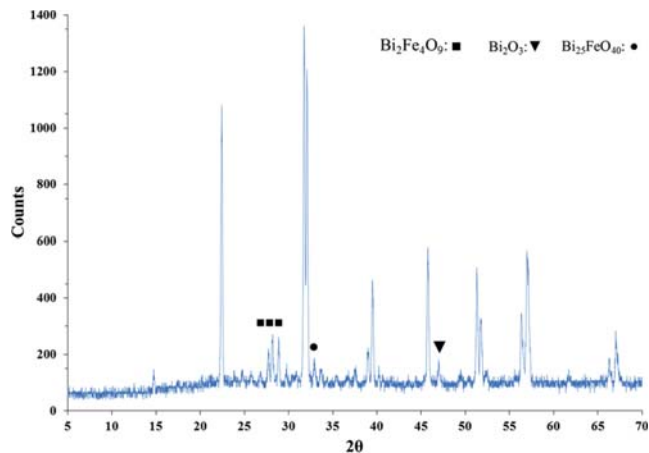

Fig. 2. XRD pattern of prepared BFO powder calcinated at 700 °C for 5 hours.

$$\text{NO Conversion \%} = \frac{[NO]_o - 2[N_2]_t}{[NO]_o} \times 100 \tag{8}$$

where $[NO]_o$ is the initial concentration of NO and $[N_2]_t$ is the concentration of N_2 in t min after irradiation.

RESULTS AND DISCUSSION

1. Characterization of Synthesized BFO Nanoparticles

Fig. 2 shows the XRD pattern of BFO nanopowder calcined at 700 °C for 5 h in the air atmosphere. According to the standard XRD data for the perovskite structure of BFO in the form of the rhombohedral (JCPDS No. 71-2494) and reported XRD pattern of perovskite type BFO [19-21], all the peaks can be indexed to BFO diffraction patterns with perovskite structure. Only some $Bi_2Fe_4O_9$, $Bi_{25}FeO_{40}$ and Bi_2O_3 impurity weak peaks were detected around $2\theta=28$, 33 and 47°, respectively. These impurities may be due to lack of control over the synthesis conditions or the volatility of bismuth and bismuth oxide species [22]. It has been reported that $Bi_2Fe_4O_9$, as a second-phase, formed above 675 °C [23]. These results confirm that the BFO relatively pure crystals can be successfully synthesized. From the Debye-Scherrer formula [24] the average crystalline size of prepared nanoparticles was calculated as 19 nm.

Fig. 3(a), (b) show the FE-SEM images of prepared BFO particles in different scale. From the FE-SEM images, low agglomeration of particles and porous structure of prepared catalyst are observed. The porous structure increases the available surface area and improves the light harvesting efficiency and causes to increase the catalytic activity [16]. Fig. 3(c) shows the surface image of immobilized BFO nanopowder on the micro slides of glass plates. As shown in Fig. 3(c), the agglomeration in the immobilized sample is seen, but the porous structure in the immobilized sample also maintains to some extent.

Fig. 4(a) shows the UV-Vis absorbance of the prepared BFO, from which the absorption edge for the prepared sample was observed around 575 nm. The absorption edge of 575 nm indicated that this photocatalyst can be excited by electromagnetic wave with wavelength less than 575 nm. Based on the UV-Vis DRS, the plotted graph of $(\alpha h\upsilon)^2$ vs. hυ (Fig. 4(b)) was used to calculate the
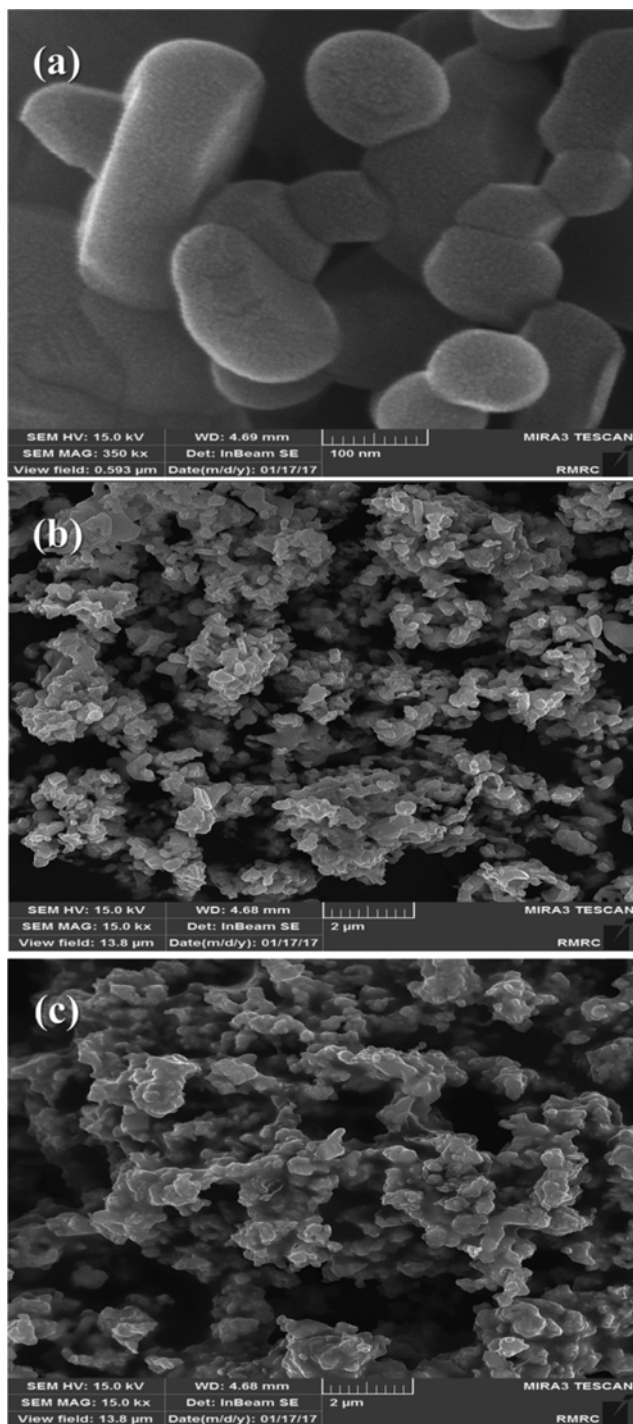
Fig. 3. FE-SEM image of (a), (b) prepared BiFeO₃ nanoparticles and (c) immobilized BFO.

Fig. 4. (a) Diffuse reflectance spectra (DRS) of BFO (b) plot of $(\alpha h\upsilon)^2$ as a function of $h\upsilon$ for determination of E_g.

frequency, Eg: band gap, and A: proportional constant. The BFO is a direct band gap semiconductor [25,26], so the value of n is 1/2. The corresponding values of band gap energy of BFO nanoparticles can be evaluated by extrapolating the linear portion of $(\alpha h\nu)^2$ versus $(h\nu)$ [25].

The BET analysis of prepared BFO nanoparticles determined that the specific surface area, average pore diameter and pore volume were 55.1 m^2/g, 1.736 nm and 0.024 cm^3/g, respectively. The specific surface area of synthesized BFO is significantly higher than similar catalysts that have been reported by Soltani et al. [27] (34.95 m^2/g) and Huo et al. [28] (28.1 m^2/g).

2. NO Removal over Immobilized BFO/UV Irradiation

Photodecomposition of NO was in 5 ppm NO, 10% relative humidity, under 8 W UV lamp irradiation, and 30 °C. Before beginning the photocatalytic test, darkness and photolysis tests were performed at the same experimental conditions. Fig. 5 shows the photocatalytic performance and adsorption behavior of synthesized BFO nanopowder that is immobilized on the micro slides glass plates in the removal of NO. The results showed that the photodecomposition of NO is negligible in the absence of the UV light (adsorption) and also in the absence of immobilized BFO plates (photolysis) no significant N_2 was detected. In contrast, when BFO

optical band gap energy of prepared BFO, in which the band gap energy of synthesized BFO was obtained 2.13 eV.

The optical absorption coefficient near the band edge follows the Tauc equation:

$$(\alpha h\nu)^{1/n} = A(h\nu - Eg) \qquad (9)$$

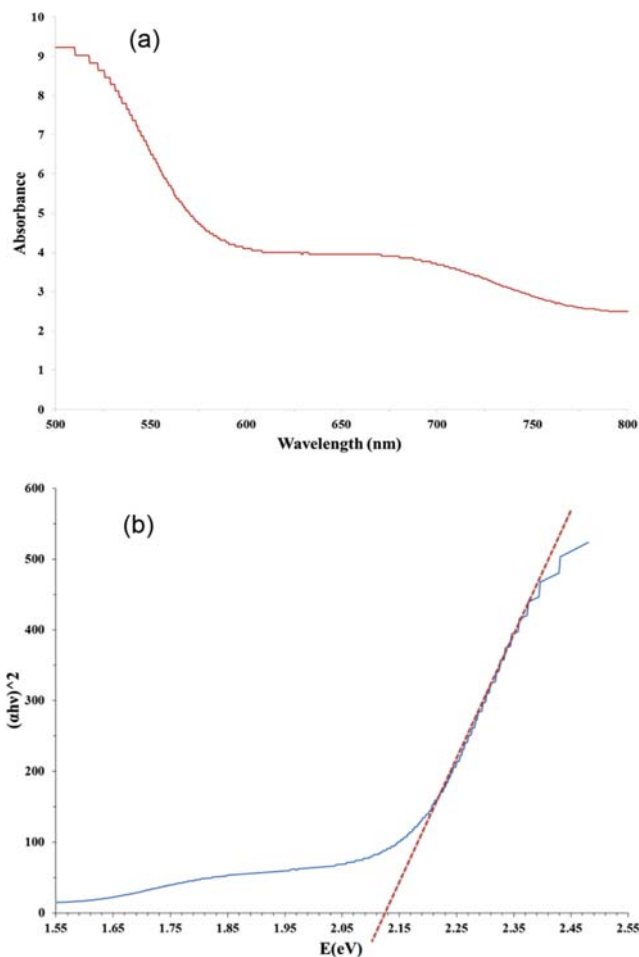where α is the absorption coefficient, h: Planck constant, ν: light
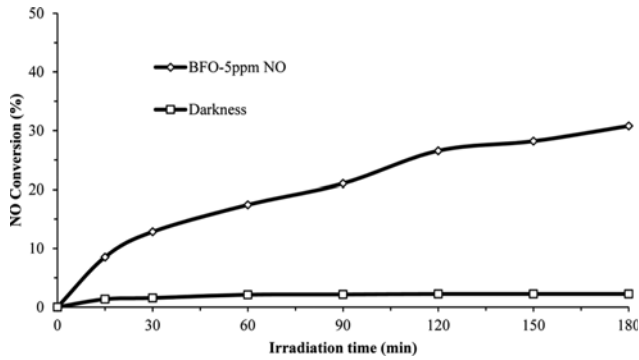
Fig. 5. BFO and UV light effect on the photocatalytic removal of NO. [NO]$_o$=5 ppmv; [BFO]=1.2 g and RH=10%.

Fig. 6. Effect of initial concentration of NO on the photocatalytic removal performance. [NO]$_o$=5-30 ppmv; [BFO]=1.2 g and RH=10%.

immobilized glass plates and irradiation were used simultaneously, as soon as the UV lamp was turned on, the concentration of the N$_2$ started to increase rapidly due to the generation of enough electron-hole pairs and start of the NO photodecomposition. Thus, the main removal of NO in the presence of UV light and BFO is attributed to the photodecomposition of NO over the immobilized BFO photocatalyst. The maximum of NO conversion to N$_2$ was obtained at 30.79%. Based on the GC/TCD analysis data, N$_2$ and O$_2$ was detected, it is concluded that NO photodecomposition is the main reaction. As a result, according to our data, as well as the other reported works, the following reactions are proposed for the this process [12]:

$$BFO+h\nu \rightarrow BFO\ (e_{CB}^- + h_{VB}^+) \tag{10}$$

$$NO\ (g) \rightarrow NO\ _{(ads)} \tag{11}$$

$$NO\ _{(ads)} + e_{CB}^- \rightarrow N\ _{(ads)} + O\ _{(ads)} \tag{12}$$

$$NO\ _{(ads)} + N\ _{(ads)} \rightarrow N_2O\ _{(ads)} \tag{13}$$

$$NO\ _{(ads)} + O\ _{(ads)} \rightarrow NO_2\ _{(ads)} \tag{14}$$

$$2N\ _{(ads)} \rightarrow N_2\ (g) \tag{15}$$

$$2O\ _{(ads)} \rightarrow O_2\ (g) \tag{16}$$

$$2NO\ _{(ads)} \rightarrow N_2\ (g) + O_2\ (g) \tag{17}$$

$$2N_2O\ _{(ads)} \rightarrow 2N_2\ (g) + O_2\ (g) \tag{18}$$
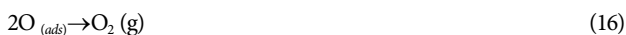
3. Effect of Initial Concentration of NO on the Photocatalytic Performance

In Iran, NOx concentration in the large cities' tunnels is about 5 ppm [29]. For consideration of the high concentration, we carried out the NOx removal process in the range of 5 to 30 ppm. Therefore, the effect of initial concentration of NO on photodecomposition rate was investigated in 5, 10, 20, and 30 ppm concentration of NO. As shown in Fig. 6, increasing the NO initial concentration causes to decrease the photocatalytic removal of NO. According to the assumption that initial adsorption of NO on the BFO controls the photocatalytic reaction; therefore, increasing the initial concentration of NO causes to saturate the adsorption sites on BFO surface and the photodecomposition rate levels out [1].

4. Effect of UV Light Power on the NO Photodecomposition

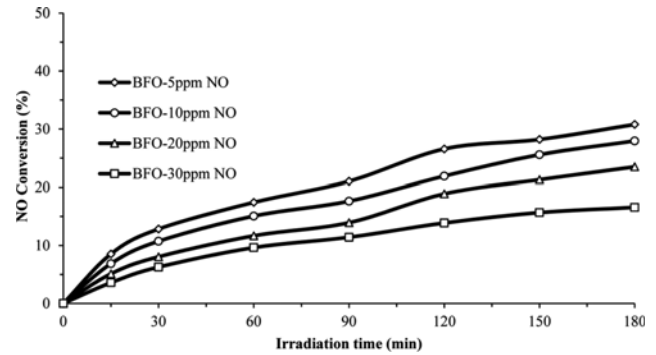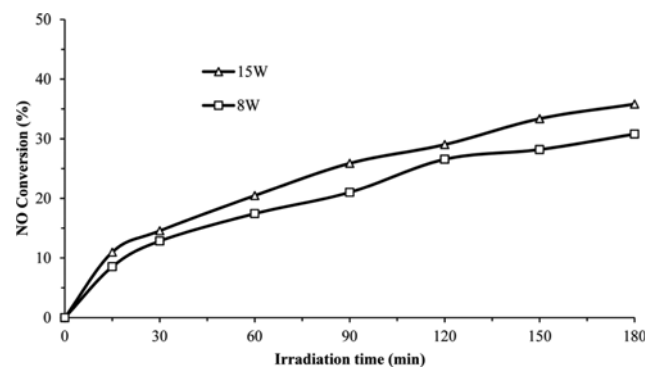The effect of UV light power on the photocatalytic removal of

Fig. 7. Effect of light power on the photocatalytic removal performance of NO. [NO]$_o$=5 ppmv; [BFO]=1.2 g and RH=10%.

NO is illustrated in Fig. 7. As shown, photocatalytic conversion of NO in the presence of 15 W UV lamp is higher than 8 W UV lamp. The UV light source is responsible for providing enough energy to excite electrons from the valence band to the conduction band and thus generating electron-hole pairs at the photocatalyst surface and thus photocatalytic process. A high UV light intensity can generate a greater amount of electron-hole pairs that cause acceleration the photodecomposition process [1]. Note that because the adsorption of pollutants on the photocatalyst surface limits the reaction rate of photodecomposition, raising the intensity of the UV lamp not always results in increasing of NO conversion [30,31].

5. Effect of BFO Dosage on the Photocatalytic Removal of NO

Generally, catalyst amount is a key factor in the initial rate of catalytic reaction and increasing the catalyst loading proportionally increases the initial rate of the photocatalytic process [32]. To assess the influence of the BFO loading amount on the NO conversion, the used photocatalyst was varied from 1.2 g (6 BFO immobilized glass plates) to 0.2 g (1 BFO immobilized glass plate). Fig. 8 shows the photocatalytic removal of NO in the presence of different loading amount of BFO photocatalyst. As expected, the photocatalytic performance of NO removal decreases with decreasing of photocatalyst amount. According to the fact that the photocatalytic reaction takes place at the surface active sites of BFO, surface-active sites decreased by decreasing the catalyst amount and subsequently conversion of NO descended [1,33].
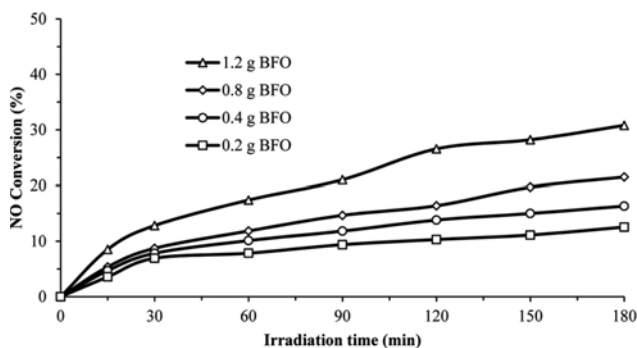
Fig. 8. Effect of BFO dosage on the photocatalytic removal performance of NO. [NO]ₒ=5 ppmv; [BFO]=0.2-1.2 g and RH=10%.

CONCLUSION

BFO nanoparticles with porous morphology and average crystalline size of 19 nm were synthesized successfully by sol-gel auto-combustion method. From the UV-Vis DRS results, band gap energy was obtained as 2.13 eV. Glass plate immobilized BFO photocatalyst successfully removed the NO pollutant from the gas phase under the UV light irradiation. NO removal efficiency was affected by the initial concentration of pollutant, catalyst loading amount, and illumination power. Increasing the catalyst loading and light intensity caused to increase the photocatalytic removal efficiency, but for increasing the initial concentration of NO, decreasing in removal efficiency was observed. Finally, the results showed that the highest conversion of 5 ppm of NOx was obtained at 35.83% under 15 W UV lamp and 1.2 g immobilized BFO.

ACKNOWLEDGEMENTS

REFERENCES

1. J. Ângelo, L. Andrade, L. M. Madeira and A. Mendes, *J. Environ. Manage.*, **129**, 522 (2013).
2. J. Lasek, Y.-H. Yu and J. Wu, *J. Photochem. Photobiol. C: Photochem. Rev.*, **14**, 29 (2013).
3. F. Normann, K. Andersson, B. Leckner and F. Johnsson, *Progress in Energy and Combustion Science*, **35**(5), 385 (2009).
4. P. N. Panahi, A. Niaei, D. Salari, S. M. Mousavi and G. Delahay, *J. Environ. Sci.*, **35**, 135 (2015).
5. S. Roy, M. Hegde and G. Madras, *Appl. Energy*, **86**(11), 2283 (2009).
6. T. Maggos, J. Bartzis, P. Leva and D. Kotzias, *Appl. Phys. A*, **89**(1), 81 (2007).
7. G. Catalan and J. F. Scott, *Adv. Mater.*, **21**(24), 2463 (2009).
8. H. Liu, Y. Guo, B. Guo and D. Zhang, *Solid State Sciences*, **19**, 69 (2013).
9. Z. Ai, W. Ho, S. Lee and L. Zhang, *Environ. Sci. Technol.*, **43**(11), 4143 (2009).
10. S. N. Habisreutinger, L. Schmidt-Mende and J. K. Stolarczyk, *Angewandte Chemie International Edition*, **52**(29), 7372 (2013).
11. M. Humayun, A. Zada, Z. Li, M. Xie, X. Zhang, Y. Qu, F. Raziq and L. Jing, *Appl. Catal. B: Environ.*, **180**, 219 (2016).
12. N. Bowering, G. S. Walker and P. G. Harrison, *Appl. Catal. B: Environ.*, **62**(3), 208 (2006).
13. M. Anpo, T.-H. Kim and M. Matsuoka, *Catal. Today*, **142**(3), 114 (2009).
14. H. Yamashita, Y. Ichihashi, S. G. Zhang, Y. Matsumura, Y. Souma, T. Tatsumi and M. Anpo, *Appl. Surf. Sci.*, **121**, 305 (1997).
15. M. Anpo and M. Takeuchi, *J. Catal.*, **216**(1), 505 (2003).
16. A. O. Ibhadon and P. Fitzpatrick, *Catalysts*, **3**(1), 189 (2013).
17. J. Schneider, M. Matsuoka, M. Takeuchi, J. Zhang, Y. Horiuchi, M. Anpo and D. W. Bahnemann, *Chem. Rev.*, **114**(19), 9919 (2014).
18. M. Fathinia, A. Khataee, M. Zarei and S. Aber, *J. Mol. Catal. A: Chem.*, **333**(1), 73 (2010).
19. C. Quan, Y. Han, N. Gao, W. Mao, J. Zhang, J. Yang and W. Huang, *Ceramics International*, **42**(1), 537 (2016).
20. N. Gao, C. Quan, Y. Ma, Y. Han, Z. Wu, W. Mao, J. Zhang, J. Yang and W. Huang, *Physica B: Condensed Matter*, **481**, 45 (2016).
21. F. Gao, X. Chen, K. Yin, S. Dong, Z. Ren, F. Yuan, T. Yu, Z. Zou and J. M. Liu, *Adv. Mater.*, **19**(19), 2889 (2007).
22. L. Li, X. Liu, Y. Zhang, P. A. Salvador and G. S. Rohrer, *Int. J. Hydrogen Energy*, **38**(17), 6948 (2013).
23. D.-C. Jia, J.-H. Xu, H. Ke, W. Wang and Y. Zhou, *J. European Ceramic Soc.*, **29**(14), 3099 (2009).
24. S. Aber, H. Mehrizade and A. R. Khataee, *Desalination Water Treatment*, **28**(1-3), 92 (2011).
25. Y. Sheng-Hong, C. Sen, Y. Ning and Z. Yue-Li, *Ferroelectrics*, **454**(1), 78 (2013).
26. H. Mehrizadeh, A. Niaei, H.-H. Tseng, D. Salari and A. Khataee, *J. Photochem. Photobiol. A: Chem.*, **332**, 188 (2017).
27. T. Soltani and B.-K. Lee, *J. Hazard. Mater.*, **316**, 122 (2016).
28. Y. Huo, Y. Jin and Y. Zhang, *J. Mole. Catal. A: Chem.*, **331**(1), 15 (2010).
29. M. A. Zazouli, A. Nattaj Jolodar and M. Hoseinei, *J. Appl. Sci. Environ. Manage.*, **12**(1), 119 (2018).
30. S. Devahasdin, C. Fan, K. Li and D. H. Chen, *J. Photochem. Photobiol. A: Chem.*, **156**(1), 161 (2003).
31. J. V. S. de Melo and G. Trichês, *Building Environ.*, **49**, 117 (2012).
32. U. I. Gaya and A. H. Abdullah, *J. Photochem. Photobiol. C: Photochem. Rev.*, **9**(1), 1 (2008).
33. G. Hüsken, M. Hunger and H. Brouwers, *Building Environ.*, **44**(12), 2463 (2009).